Research Article **Open Access**

Tasawar Hayat, Muhammad Farooq*, and Ahmed Alsaedi

Stagnation point flow of carbon nanotubes over stretching cylinder with slip conditions

Abstract: This work concentrates on stagnation point flow of a nanofluid over an impermeable stretching cylinder with mass transfer and slip effects. Carbon nanotubes (CNTs) and water are used as a nanofluid in the present investigation. Two types of CNTs are used as nanoparticles (i) Single-wall carbon nanotubes (SWCNTs) and (ii) multi-wall carbon nanotubes (MWCNTs). Appropriate transformations are used to achieve a system of ordinary differential equations. Convergent series solutions are obtained. Behavior of various parameters on the velocity, temperature and concentration profiles are discussed graphically. Numerical values of skin friction coefficient, Nusselt number and Sherwood number are computed and analyzed.

Keywords: stagnation point; Carbon nanotubes; slip effects; mass transfer

PACS: 44.10.+i, 44.20.+b, 44.27.+g, 47.15.Cb

DOI 10.1515/phys-2015-0024
Received October 22, 2014; accepted January 26, 2015

1 Introduction

In recent years development of human society greatly depends on the energy resources. Researchers and scientists are interested in exploring new energy resources and energy technologies in order to utilize solar energy (which when it reaches the earth is about $4x10^{15}$MW). This solar energy is 2000 times larger than the global energy consumption. Nano material (nano particles) was used for the first time by Choi [1]to enhance thermal conductivity of fluids and storage of energy. Solar thermal energy is very suitable, easily available and a friendly source for various heating processes in industries and technologies. Such processes cannot rely on energy of limited resources. A solar collector is a device which is used to convert solar radiation into heat energy. This heat energy is absorbed by the existing material in the solar collector. Solar energy can be used to heat water but the difficulty of such technology is that it has low efficiency because water is used as an energy carrier in solar collectors. Water has a low heat transfer coefficient due to poor thermophysical properties. Therefore to enhance the efficiency of such collectors, a new class of fluids known as nanofluids has been investigated (see Said *et al.* [2]). A nanofluid is a mixture of a base fluid and nanoparticles. It is used to enhance the rate of heat transfer of microelectronics, microchips in computers, fuel cells, transportation, biomedicine, food processing, solid state lightening and manufacturing. Most liquids such as water, ethylene, glycol oil *etc.* have low thermal conductivity. To increase the thermal conductivity of such materials suspended nano sized metallic particles (titanium, copper, gold, iron or their oxides) are used in the fluids. Nanoparticles have various shapes for example spherical, rod-like or tubular. Rashidi *et al.* [3] examined magnetohydrodynamic flow of a nanofluid induced by a rotating porous disk with entropy generation. Sheikholeslami *et al.* [4] presented heat transfer analysis of nanofluid saturated with porous medium past a permeable stretching wall. Analysis of nanofluid past an exponentially permeable sheet was investigated by Bhattacharyya and Layek [5]. Natural convection flow of nanofluid with thermal management was studied by Sheikholeslami *et al.* [6]. Characteristics of mixed convection and Newtonian heating on flow of nanofluid were examined by Imtiaz *et al.* [7]. Turkyilmazoglu [8] examined unsteady boundary layer flow of nanofluid over a vertical flat plate.

Analysis of stagnation point flow is still the main focus of researchers and scientists due to its many applications in engineering and industries. Such flows may be inviscid or viscous, two-dimensional or three-dimensional, symmetric or asymmetric, steady or unsteady, normal or oblique, forward or reverse, homogeneous or two immiscible fluids (see Weidman and Putkaradze [9]). Further such flows become more important in the presence of stretching/shrinking of the surface due to widespread ap-

***Corresponding Author: Muhammad Farooq:** Department of Mathematics, Quaid-I-Azam University 45320, Islamabad 44000, Pakistan, E-mail: hfarooq99@yahoo.com
Tasawar Hayat: Department of Mathematics, Quaid-I-Azam University 45320, Islamabad 44000, Pakistan
Ahmed Alsaedi: Nonlinear Analysis and Applied Mathematics (NAAM) Research Group, Department of Mathematics, Faculty of Science, King Abdulaziz University, P. O. Box 80257, Jeddah 21589, Saudi Arabia

plications in engineering and industrial processes. Such processes involve glass fibre production, hot rolling, wire drawing, metal and polymer extrusion, continuous casting *etc*. [10, 11]. Linear stretching is important in the process of extrusion from a die. Bhattacharyya and Vajravelu [12] presented boundary layer stagnation point flow over an exponentially shrinking sheet. Turkyilmazoglu and Pop [13] analyzed stagnation point flow of a Jeffrey fluid induced by a stretching/shrinking sheet. Hayat *et al*. [14] investigated boundary layer stagnation point flow of an Oldroyd-B fluid with thermal stratification due to a linear stretching sheet. Mukhopadhyay [15] analyzed radiative stagnation point flow past a permeable stretching sheet with variable viscosity.

Most researchers investigated boundary layer flow of a nanofluid over a stretching sheet using Cu, Ag, Al_2O_3 nanoparticles. Our main objective is to analyze the behavior of a base fluid (water) with single and multi-wall carbon nanotubes (SWCNT and MWCNT) over a stretching cylinder. The flow analysis is carried out in the region of a stagnation point. The partial slip condition holds in the present analysis. The surface of the cylinder is subjected to variable temperature and concentration. Series solutions are developed using the homotopy analysis method [16–23]. Influence of various parameters on the skin friction coefficient, Nusselt and Sherwood numbers are explored numerically. Comparison is also made for the skin friction coefficient in the limiting case (i.e., flow of viscous fluid past a stretching flat plate without nanoparticles and slip effects). Excellent agreement is achieved.

2 Mathematical formulation

Consider steady stagnation point flow of a nanofluid by a stretching cylinder with slip conditions. Analysis of mass transfer is also carried out. Single and multi-wall carbon nanotubes are used as nanoparticles and water is a base fluid. Cylindrical coordinates are chosen in such a way that the x-axis is along the axial direction of the cylinder while the r-axis is normal to it. Temperature ($T_w(x) = T_0 + a\,(x/l)$) and concentration ($C_w(x) = C_0 + b\,(x/l)$) are assumed to vary linearly at the surface of the cylinder. This occurs in the processes of wire drawing, metal and polymer extrusion *etc*. Here linear stretching occurs and also distributions of temperature and concentration are linear [11]. Stretching velocity of the cylinder is produced by applying two forces equal in magnitude but opposite in direction. Using boundary layer approximations ($o(x) = o(u) = o(1),\ o(r) = o(v) = o(\delta)$), the conservation laws are reduced to the following forms

$$\frac{\partial (rv)}{\partial r} + \frac{\partial (ru)}{\partial x} = 0, \tag{1}$$

$$v\frac{\partial u}{\partial r} + u\frac{\partial u}{\partial x} = U_e\frac{dU_e}{dx} + \nu_{nf}\left(\frac{\partial^2 u}{\partial r^2} + \frac{1}{r}\frac{\partial u}{\partial r}\right), \tag{2}$$

$$u\frac{\partial T}{\partial x} + v\frac{\partial T}{\partial r} = \alpha_{nf}\left(\frac{\partial^2 T}{\partial r^2} + \frac{1}{r}\frac{\partial T}{\partial r}\right), \tag{3}$$

$$u\frac{\partial C}{\partial x} + v\frac{\partial C}{\partial r} = D\left(\frac{\partial^2 C}{\partial r^2} + \frac{1}{r}\frac{\partial C}{\partial r}\right). \tag{4}$$

Boundary conditions are

$$\begin{aligned} &u = U_w(x) + L\frac{\partial u}{\partial r},\quad v = 0,\quad T = T_w(x) + K_1\frac{\partial T}{\partial r},\\ &C = C_w(x) + K_2\frac{\partial C}{\partial r}\ \text{ at } r = R,\end{aligned}$$

$$u \to U_e(x) = \frac{U_\infty x}{l},\quad T \to T_\infty,\ C \to C_\infty\ \text{ as } r \to \infty. \tag{5}$$

In the above expressions u and v denote velocity components in the axial and radial directions respectively, R is the radius of a cylinder, U_w and U_e are stretching and free stream velocities respectively, ν_{nf} is kinematic viscosity of the nanofluid, α_{nf} is thermal diffusivity of the nanofluid, D is mass diffusivity, L, K_1 and K_2 are the slip coefficients for velocity, thermal and concentration respectively, T and C are temperature and concentration of the fluid respectively, l is characteristic length, ρ is density, T_w and C_w are temperature and concentration at the surface respectively, T_∞ and C_∞ are temperature and concentration away from the surface respectively, a and b are dimensional constants, T_0 and C_0 are reference temperature and concentration respectively.

We write

$$\begin{aligned} \mu_{nf} &= \frac{\mu_f}{(1-\phi)^{2.5}},\quad \rho_{nf} = (1-\phi)\rho_f + \phi\rho_s\,(c_p)_{CNT},\\ \alpha_{nf} &= \frac{k_{nf}}{\rho_{nf}\,(c_p)_{nf}},\\ \frac{k_{nf}}{k_f} &= \frac{(1-\phi) + 2\phi\frac{k_{CNT}}{k_{CNT}-k_f}\ln\frac{k_{CNT}+k_f}{2k_f}}{(1-\phi) + 2\phi\frac{kf}{k_{CNT}-k_f}\ln\frac{k_{CNT}+k_f}{2k_f}}, \end{aligned} \tag{6}$$

where μ_{nf} is viscosity of nanofluid, ϕ is nanoparticle volume fraction, ρ_f and ρ_s are density of the fluid and solid particles respectively, k_f and k_{nf} are thermal conductivities of fluid and nanomaterial respectively.

Table 1: Thermophysical properties of base fluid and nanoparticles [24].

Physical Properties	Base fluid	Nanoparticles	
	Water	SWCNT	MWCNT
$\rho\,(kg/m^3)$	997	2600	1600
$c_p\,(J/kgK)$	4179	425	796
$k\,(W/mK)$	0.613	6600	3000

Transformations are defined as follows:

$$\begin{aligned} \eta &= \sqrt{\frac{U_0}{\nu_f l}}\left(\frac{r^2-R^2}{2R}\right), \quad \psi = \sqrt{U_w \nu_f x} R f(\eta) \\ u &= \frac{U_0 x}{l} f'(\eta),\ v = -\sqrt{\frac{\nu U_0}{l}}\frac{R}{r} f(\eta), \\ \theta(\eta) &= \frac{T-T_\infty}{T_w-T_\infty}, \quad \varphi(\eta) = \frac{C-C_\infty}{C_w-C_\infty}. \end{aligned} \tag{7}$$

The incompressibility condition is satisfied automatically and Equations (2) to (5) are reduced to

$$\left(\frac{1}{(1-\phi)^{2.5}\left(1-\phi+\phi\frac{\rho_{CNT}}{\rho_f}\right)}\right)\left((1+2\gamma\eta)f''' + 2\gamma f''\right) + f f'' - \left(f'\right)^2 + A^2 = 0, \tag{8}$$

$$\left(\frac{k_{nf}/k_f}{\left(1-\phi+\phi\frac{(\rho c_p)_{CNT}}{(\rho c_p)_f}\right)}\right)\left((1+2\gamma\eta)\theta'' + 2\gamma\theta'\right) + \Pr\left(f\theta' - f'\theta\right) = 0, \tag{9}$$

$$(1+2\gamma\eta)\varphi'' + 2\gamma\varphi' + Sc\left(f\varphi' - f'\varphi\right) = 0. \tag{10}$$

The boundary conditions take the form

$$\begin{aligned} f(0) &= 0,\ f'(0) = 1 + S_1 f''(0), \\ \theta(0) &= 1 + S_2\theta'(0),\ \varphi(0) = 1 + S_3\varphi'(0) \\ f'(\infty) &= A,\ \theta(\infty) = 0,\ \varphi(\infty) = 0, \end{aligned} \tag{11}$$

where γ is the curvature parameter, A is the ratio of velocities, Pr is the Prandtl number, S_1, S_2 and S_3 are the velocity, thermal and solutal slip parameters and Sc is the Schmidt number. These quantities are defined as follows:

$$\begin{aligned} \gamma &= \left(\frac{\nu l}{U_0 R^2}\right)^{1/2},\ \Pr = \frac{\mu c_p}{k},\ A = \frac{U_\infty}{U_0},\ Sc = \frac{\nu}{D}, \\ S_1 &= L\sqrt{\frac{U_0}{\nu l}},\ S_2 = K_1\sqrt{\frac{U_0}{\nu l}},\ S_3 = K_2\sqrt{\frac{U_0}{\nu l}}. \end{aligned} \tag{12}$$

The skin friction coefficient, local Nusselt and Sherwood numbers are

$$C_f = \frac{\tau_w}{\rho_f U_w^2},\ Nu_x = \frac{x q_w}{k_f(T_w - T_\infty)},\ Sh = \frac{x j_w}{D(C_w - C_\infty)},$$

$$\tau_w = \mu_{nf}\left(\frac{\partial u}{\partial r}\right)_{r=R},\ q_w = -\kappa_{nf}\left(\frac{\partial T}{\partial r}\right)_{r=R}, \quad j_w = -D\left(\frac{\partial C}{\partial r}\right)_{r=R}. \tag{13}$$

The skin friction, local Nusselt number and Sherwood number in dimensionless form are

$$C_f Re_x^{1/2} = \frac{1}{(1-\phi)^{2.5}} f''(0), \quad Nu_x Re_x^{-1/2} = -\frac{k_{nf}}{k_f}\theta'(0), \quad Sh Re_x^{-1/2} = -\varphi'(0), \tag{14}$$

where $Re_x = U_w l/\nu$ is the Reynolds number.

3 Homotopic solutions

Homotopy analysis method provides great freedom to choose the initial guess and linear operators. Initial guess is selected in such a way that boundary conditions are satisfied while linear operator is the linear part of the equation. Thus we have

$$\begin{aligned} f_0(\eta) &= A\eta + \frac{(1-A)}{(1+S_1)}\left(1-\exp(-\eta)\right), \\ \theta_0(\eta) &= \frac{1}{1+S_2}\exp(-\eta),\ \varphi_0(\eta) = \frac{1}{1+S_3}\exp(-\eta), \end{aligned} \tag{15}$$

$$\mathcal{L}_f(f) = \frac{d^3 f}{d\eta^3} - \frac{df}{d\eta}, \quad \mathcal{L}_\theta(\theta) = \frac{d^2\theta}{d\eta^2} - \theta, \quad \mathcal{L}_\varphi(\varphi) = \frac{d^2\varphi}{d\eta^2} - \varphi, \tag{16}$$

with

$$\mathcal{L}_f\left[A_1 + A_2\exp(\eta) + A_3\exp(-\eta)\right] = 0, \tag{17}$$

$$\mathcal{L}_\theta\left[A_4\exp(\eta) + A_5\exp(-\eta)\right] = 0, \tag{18}$$

$$\mathcal{L}_\varphi\left[A_6\exp(\eta) + A_7\exp(-\eta)\right] = 0, \tag{19}$$

where $A_i\,(i = 1-5)$ are arbitrary constants. The zeroth and mth order deformation problems are

3.1 Zeroth-order problem

$$(1-p)\mathcal{L}_f\left[\widehat{f}(\eta;p) - f_0(\eta)\right] = p\hbar_f\mathcal{N}_f\left[\widehat{f}(\eta;p)\right], \tag{20}$$

$$(1-p)\mathcal{L}_\theta\left[\widehat{\theta}(\eta;p) - \theta_0(\eta)\right] = p\hbar_\theta\mathcal{N}_\theta\left[\widehat{\theta}(\eta;p), \widehat{f}(\eta;p)\right], \tag{21}$$

$$(1-p)\mathcal{L}_\varphi\left[\widehat{\varphi}(\eta;p) - \varphi_0(\eta)\right] = p\hbar_\varphi\mathcal{N}_\varphi\left[\widehat{\varphi}(\eta;p), \widehat{f}(\eta;p)\right], \tag{22}$$

$$\widehat{f}(0;p)=0,\quad \widehat{f}'(0;p)=1+S_1\widehat{f}''(0;p),\quad \widehat{f}'(\infty;p)=A, \tag{23}$$

$$\begin{aligned}&\widehat{\theta}(0;p)=1+S_2\widehat{\theta}'(0;p),\quad &&\widehat{\theta}(\infty;p)=0,\\ &\widehat{\varphi}(0;p)=1+S_3\widehat{\varphi}'(0;p),\quad &&\widehat{\varphi}(\infty;p)=0,\end{aligned} \tag{24}$$

$$\begin{aligned}&\mathcal{N}_f\left[\widehat{f}(\eta,p),\widehat{\theta}(\eta;p),\widehat{\varphi}(\eta;p)\right]\\ &=\left(\frac{1}{(1-\phi)^{2.5}\left(1-\phi+\phi\frac{\rho_{CNT}}{\rho_f}\right)}\right)\left((1+2\gamma\eta)\frac{\partial^3\widehat{f}(\eta;p)}{\partial\eta^3}+2\gamma\frac{\partial^2\widehat{f}(\eta;p)}{\partial\eta^2}\right)\\ &+\widehat{f}(\eta;p)\frac{\partial^2\widehat{f}(\eta;p)}{\partial\eta^2}-\left(\frac{\partial\widehat{f}(\eta;p)}{\partial\eta}\right)^2+A^2,\end{aligned} \tag{25}$$

$$\begin{aligned}&\mathcal{N}_\theta\left[\widehat{\theta}(\eta;p),\widehat{f}(\eta;p)\right]=\left(\frac{k_{nf}/k_f}{\left(1-\phi+\phi\frac{(\rho c_p)_{CNT}}{(\rho c_p)_f}\right)}\right)\\ &\times\left((1+2\gamma\eta)\frac{\partial^2\widehat{\theta}(\eta,p)}{\partial\eta^2}+2\gamma\frac{\partial\widehat{\theta}(\eta,p)}{\partial\eta}\right)\\ &+\Pr\left(\widehat{f}(\eta;p)\frac{\partial\widehat{\theta}(\eta;p)}{\partial\eta}-\frac{\partial\widehat{f}(\eta;p)}{\partial\eta}\widehat{\theta}(\eta,p)\right),\end{aligned} \tag{26}$$

$$\begin{aligned}&\mathcal{N}_\phi\left[\widehat{\varphi}(\eta;p),\widehat{f}(\eta;p)\right]\\ &=(1+2\gamma\eta)\frac{\partial^2\widehat{\varphi}(\eta,p)}{\partial\eta^2}+2\gamma\frac{\partial\widehat{\varphi}(\eta,p)}{\partial\eta}\\ &+Sc\left(\widehat{f}(\eta;p)\frac{\partial\widehat{\varphi}(\eta;p)}{\partial\eta}-\frac{\partial\widehat{f}(\eta;p)}{\partial\eta}\widehat{\varphi}(\eta,p)\right),\end{aligned} \tag{27}$$

where $p\in[0,1]$ is embedding parameter and $\hbar_f$, $\hbar_\theta$ and $\hbar_\phi$ are non-zero auxiliary parameters.

3.2 *m*th-order deformation problems

$$\mathcal{L}_f\left[f_m(\eta)-\chi_m f_{m-1}(\eta)\right]=\hbar_f\mathcal{R}_m^f(\eta), \tag{28}$$

$$\mathcal{L}_\theta\left[\theta_m(\eta)-\chi_m\theta_{m-1}(\eta)\right]=\hbar_\theta\mathcal{R}_m^\theta(\eta), \tag{29}$$

$$\mathcal{L}_\varphi\left[\varphi_m(\eta)-\chi_m\varphi_{m-1}(\eta)\right]=\hbar_\varphi\mathcal{R}_m^\varphi(\eta), \tag{30}$$

$$f_m(0)=0,\quad f_m'(0)=S_1f_m''(0),\quad f_m'(\infty)=0, \tag{31}$$

$$\begin{aligned}&\theta_m(0)=S_2\theta_m'(0),\quad &&\theta_m(\infty)=0,\\ &\varphi_m(0)=S_3\varphi_m'(0),\quad &&\phi_m(\infty)=0.\end{aligned} \tag{32}$$

$$\begin{aligned}&\mathcal{R}_m^f(\eta)\\ &=\left(\frac{1}{(1-\phi)^{2.5}\left(1-\phi+\phi\frac{\rho_{CNT}}{\rho_f}\right)}\right)\left((1+2\gamma\eta)f_{m-1}'''+2\gamma f_{m-1}''\right)\\ &+\sum_{k=0}^{m-1}\left(f_{m-1-k}f_k''-f_{m-1-k}'f_k'\right)+A^2(1-\chi_m),\end{aligned} \tag{33}$$

$$\begin{aligned}&\mathcal{R}_m^\theta(\eta)\\ &=\left(\frac{k_{nf}/k_f}{\left(1-\phi+\phi\frac{(\rho c_p)_{CNT}}{(\rho c_p)_f}\right)}\right)\left((1+2\gamma\eta)\theta_{m-1}''+2\gamma\theta_{m-1}'\right)\\ &+\Pr\sum_{k=0}^{m-1}\left(f_{m-1-k}\theta_k'-f_{m-1-k}'\theta_k\right),\end{aligned} \tag{34}$$

$$\begin{aligned}&\mathcal{R}_m^\varphi(\eta)=(1+2\gamma\eta)\varphi_{m-1}''+2\gamma\varphi_{m-1}'\\ &+Sc\sum_{k=0}^{m-1}\left(f_{m-1-k}\varphi_k'-f_{m-1-k}'\varphi_k\right),\end{aligned} \tag{35}$$

$$\chi_m=\begin{cases}0, & m\le 1\\ 1, & m>1\end{cases}. \tag{36}$$

For $p=0$ and $p=1$, we can write

$$\widehat{f}(\eta;0)=f_0(\eta),\quad \widehat{f}(\eta;1)=f(\eta), \tag{37}$$

$$\begin{aligned}&\widehat{\theta}(\eta;0)=\theta_0(\eta),\quad \widehat{\theta}(\eta;1)=\theta(\eta),\\ &\widehat{\varphi}(\eta;0)=\varphi_0(\eta),\quad \widehat{\varphi}(\eta;1)=\varphi(\eta)\end{aligned} \tag{38}$$

and with variation of p from 0 to 1, $\widehat{f}(\eta;p)$, $\widehat{\theta}(\eta;p)$ and $\widehat{\varphi}(\eta;p)$ vary from initial solutions $f_0(\eta)$, $\theta_0(\eta)$ and $\varphi_0(\eta)$ to final solutions $f(\eta)$, $\theta(\eta)$ and $\phi(\eta)$ respectively. By Taylor's series we have

$$\begin{aligned}&\widehat{f}(\eta;p)=f_0(\eta)+\sum_{m=1}^{\infty}f_m(\eta)p^m,\\ &f_m(\eta)=\left.\frac{1}{m!}\frac{\partial^m\widehat{f}(\eta;p)}{\partial p^m}\right|_{p=0},\end{aligned} \tag{39}$$

$$\begin{aligned}&\widehat{\theta}(\eta;p)=\theta_0(\eta)+\sum_{m=1}^{\infty}\theta_m(\eta)p^m,\\ &\theta_m(\eta)=\left.\frac{1}{m!}\frac{\partial^m\widehat{\theta}(\eta;p)}{\partial p^m}\right|_{p=0},\end{aligned} \tag{40}$$

$$\begin{aligned}&\widehat{\varphi}(\eta;p)=\varphi_0(\eta)+\sum_{m=1}^{\infty}\varphi_m(\eta)p^m,\\ &\varphi_m(\eta)=\left.\frac{1}{m!}\frac{\partial^m\widehat{\varphi}(\eta;p)}{\partial p^m}\right|_{p=0}.\end{aligned} \tag{41}$$

The value of the auxiliary parameter is chosen in such a way that the series (39) to (41) converge at $p = 1$ i.e.

$$f(\eta) = f_0(\eta) + \sum_{m=1}^{\infty} f_m(\eta), \tag{42}$$

$$\theta(\eta) = \theta_0(\eta) + \sum_{m=1}^{\infty} \theta_m(\eta), \tag{43}$$

$$\varphi(\eta) = \varphi_0(\eta) + \sum_{m=1}^{\infty} \varphi_m(\eta). \tag{44}$$

The general solutions $(f_m, \theta_m, \varphi_m)$ of Equations (28)–(30) in terms of special solutions $\left(f_m^{\star}, \theta_m^{\star}, \varphi_m^{\star}\right)$ are given by

$$f_m(\eta) = f_m^{\star}(\eta) + A_1 + A_2 e^{\eta} + A_3 e^{-\eta}, \tag{45}$$

$$\theta_m(\eta) = \theta_m^{\star}(\eta) + A_4 e^{\eta} + A_5 e^{-\eta}, \tag{46}$$

$$\varphi_m(\eta) = \varphi_m^{\star}(\eta) + A_6 e^{\eta} + A_7 e^{-\eta}, \tag{47}$$

where constants A_i $(i = 1 - 5)$ through the boundary conditions (31) and (32) have values

$$\begin{aligned}
A_2 &= A_4 = A_6 = 0,\\
A_3 &= \left(\frac{1}{1+S_1}\right)\left(f_m^{\star'}(0) - S_1 f_m^{\star''}(0)\right)\\
A_1 &= -A_3 - f_m^{\star}(0)\\
A_5 &= \left(\frac{1}{1+S_2}\right)\left(S_2\theta_m^{\star\prime}(0) - \theta_m^{\star}(0)\right),\\
A_7 &= \left(\frac{1}{1+S_3}\right)\left(S_3\varphi_m^{\star\prime}(0) - \varphi_m^{\star}(0)\right).
\end{aligned} \tag{48}$$

3.3 Convergence analysis

Liao [16] in 1992 proposed homotopy analysis technique for the series solutions of highly nonlinear problems. It provides great freedom to adjust and control the convergence region of series solutions. Therefore, we have plotted the $\hbar$-curves in Figures 1 and 2. The admissible ranges of the auxiliary parameters $\hbar_f$, $\hbar_\theta$ and $\hbar_\varphi$ for the SWCNT case are $-1.3 \le \hbar_f \le -0.1$, $-0.38 \le \hbar_\theta \le -0.2$ and $-1.3 \le \hbar_\varphi \le -0.3$ while for the MWCNT case these are $-1.15 \le \hbar_f \le -0.25$, $-0.3 \le \hbar_\theta \le -0.18$ and $-1.3 \le \hbar_\varphi \le -0.25$ when $\gamma = 0.2$, $A = 0.1$, $Sc = 1.3$, $S_1 = 0.1$, $S_2 = 0.2$ and $S_3 = 0.2$.

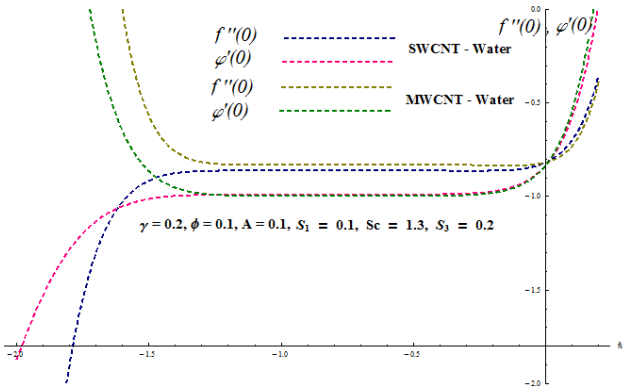

Figure 1: $\hbar$-curves for $f''(0)$ and $\varphi'(0)$.

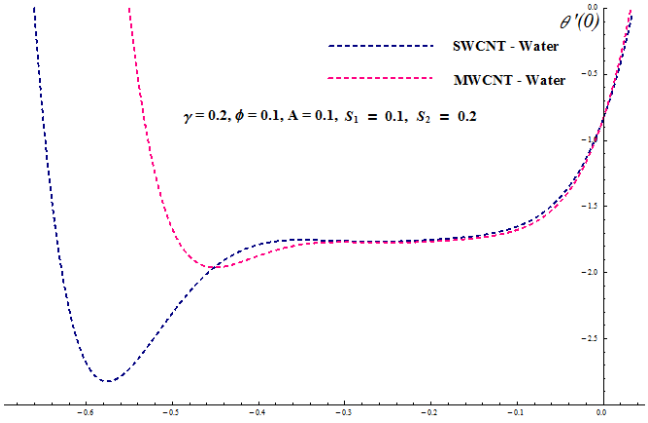

Figure 2: $\hbar$-curves for $\theta'(0)$.

These are numerical values of the $\hbar$-curves for any fixed value of the auxiliary parameter $\hbar$ selected from the convergence region (see Figures 1 and 2 and these values ensure the convergence of series solutions.

3.4 Discussion

In this section we examine the behavior of pertinent parameters on velocity, temperature and concentration profiles for single-wall and multi-wall carbon nanotubes. The influence of A on velocity profile for SWCNT and MWCNT is presented in Figure 3. The velocity profile increases for $A > 1$ and $A < 1$ while boundary layer thickness has opposite effects. For $A = 1$, there is no boundary layer because fluid and cylinder move with the same velocity. Velocity profile overlaps for both SWCNT and MWCNT. Behavior of curvature parameter γ on the velocity profile is displayed in Figure 4. The velocity profile decreases near the surface of cylinder while increases far away from the surface. However velocity profile is higher for multi-wall car-

Table 2: Convergence of series solutions for different order of approximations when $\gamma = 0.2$, $A = 0.1$, $Sc = 1.3$, $S_1 = 0.1$, $S_2 = 0.2$ and $S_3 = 0.2$.

	SWCNT			MWCNT		
Order of approximations	$-f''(0)$	$-\theta'(0)$	$-\varphi'(0)$	$-f''(0)$	$-\theta'(0)$	$-\varphi'(0)$
1	0.86277	1.1902	0.94481	0.84069	1.1905	0.94481
5	0.86153	1.6780	0.98826	0.83048	1.6868	0.99526
10	0.86123	1.7518	0.98894	0.83022	1.7602	0.99593
13	0.86122	1.7631	0.98896	0.83022	1.7715	0.99593
20	0.86122	1.7687	0.98896	0.83022	1.7771	0.99593
25	0.86122	1.7687	0.98896	0.83022	1.7771	0.99593
30	0.86122	1.7687	0.98896	0.83022	1.7771	0.99593

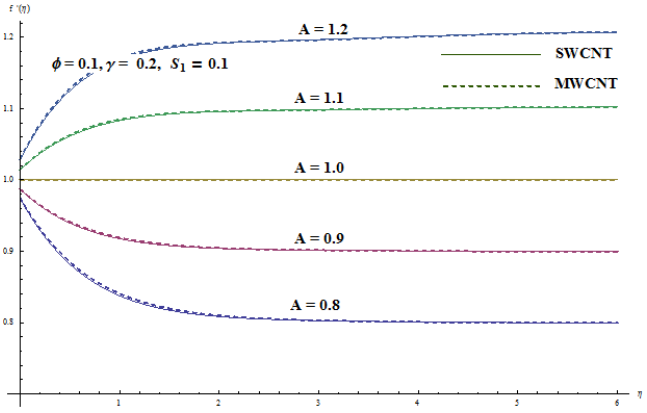

Figure 3: Effect of A on f'.

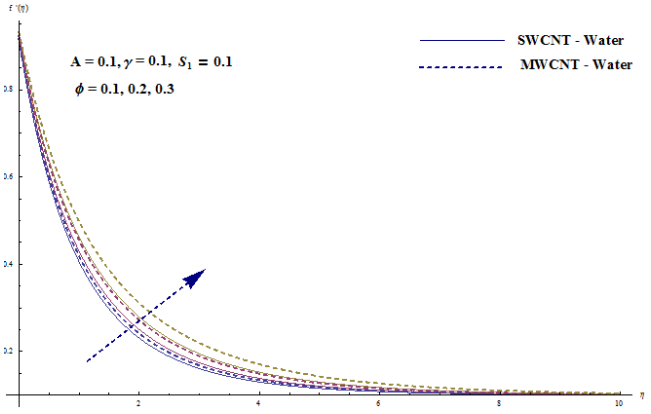

Figure 5: Effect of ϕ on f'.

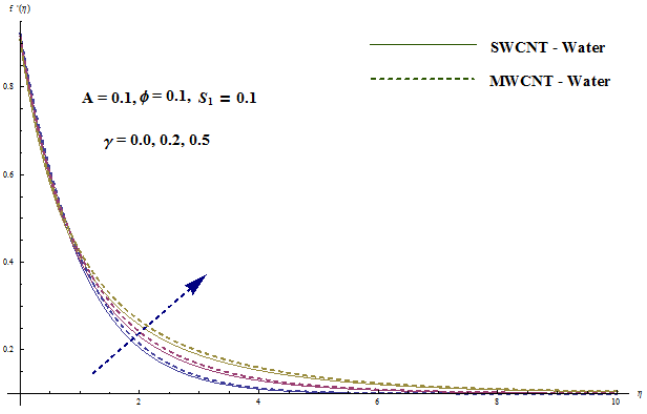

Figure 4: Effect of γ on f'.

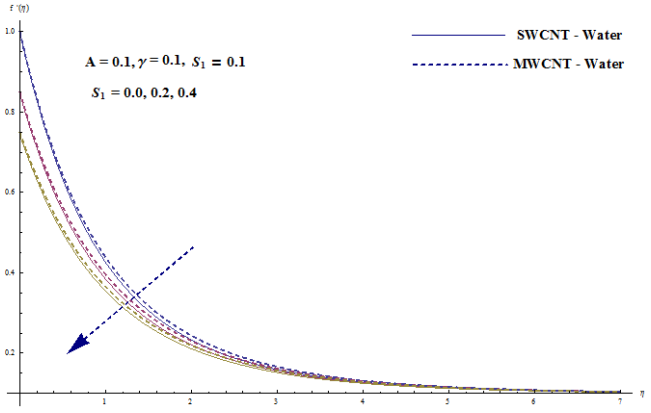

Figure 6: Effect of S_1 on f'.

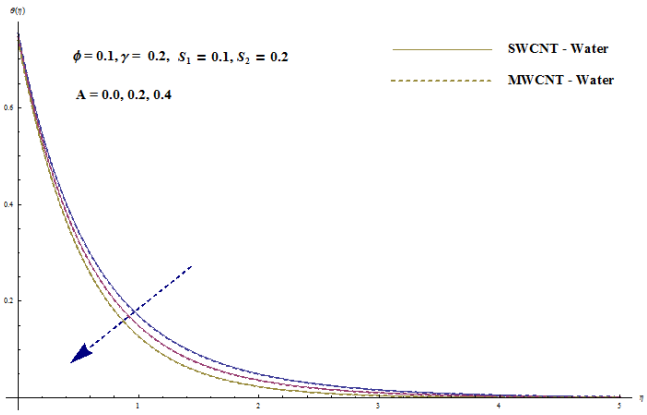

Figure 7: Effect of A on θ.

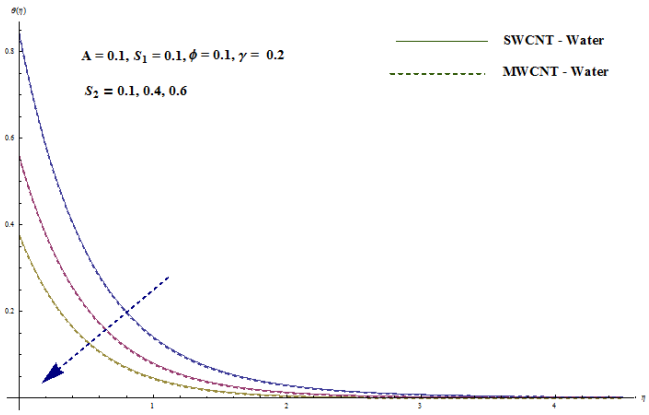

Figure 10: Effect of S_2 on θ.

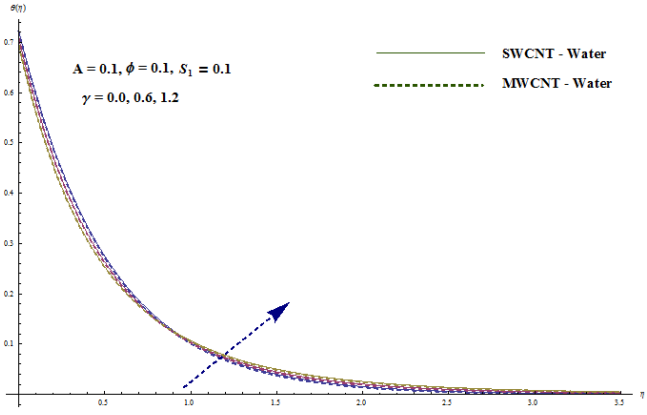

Figure 8: Effect of γ on θ.

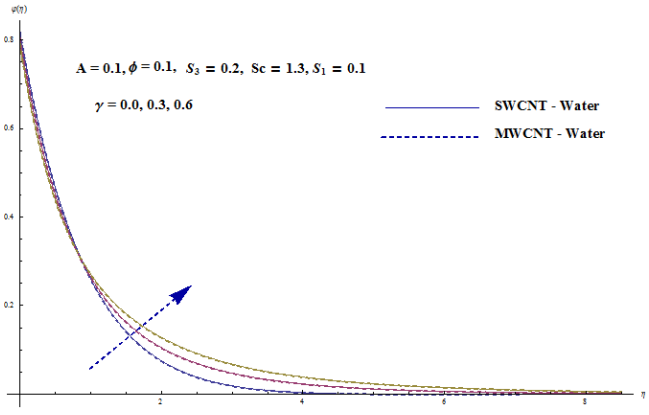

Figure 11: Effect of γ on φ.

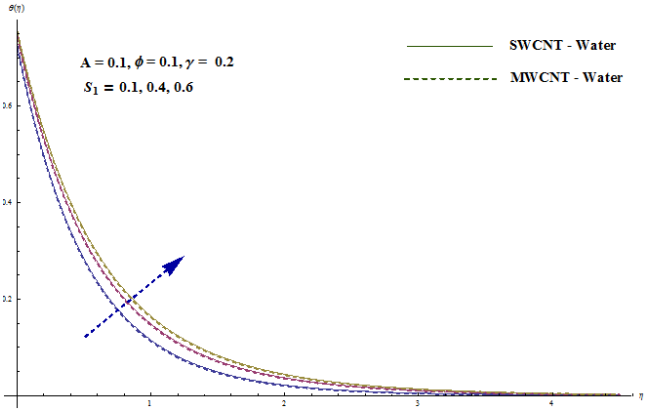

Figure 9: Effect of S_1 on θ.

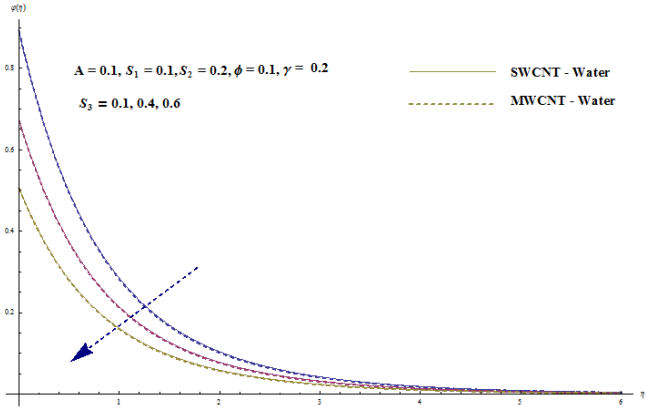

Figure 12: Effect of S_3 on φ.

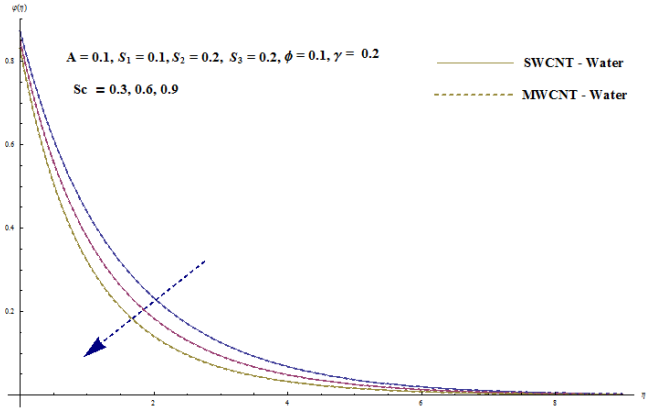

Figure 13: Effect of Sc on φ.

Table 3: Numerical values of skin friction coefficient for different parameters.

γ	A	ϕ	S_1	$-\frac{1}{(1-\phi)^{2.5}}f''(0)$	
				SWCNTs	MWCNTs
0	0.1	0.1	0.1	1.0463	1.0056
0.3				1.1578	1.1168
0.5				1.2269	1.1855
	0			1.2833	1.2247
	0.1			1.2269	1.1855
	0.3			1.0638	1.0292
	0.1	0.0		0.9817	0.9817
		0.15		1.3793	1.3113
		0.2		1.5588	1.4585
		0.1	0.1	1.2269	1.1855
			0.2	1.0858	1.0520
			0.4	0.8874	0.8645

Table 4: Numerical values of Nusselt number for different parameters when $S_1 = 0.1$.

γ	A	ϕ	S_2	$-\frac{k_{nf}}{kf}\theta'(0)$	
				SWCNTs	MWCNTs
0.0	0.2	0.1	0.2	1.7495	1.7724
0.3				1.7939	1.8019
0.5				1.8229	1.8305
	0.0			1.8044	1.8126
	0.2			1.8229	1.8305
	0.5			1.8700	1.8767
	0.2	0.0		1.8607	1.8607
		0.1		1.8229	1.8305
		0.2		1.7847	1.7985
		0.1	0.0	2.8693	2.8880
			0.2	1.8229	1.8305
			0.5	1.1785	1.3399

Table 5: Numerical values of Sherwood number for different parameters when $A = 0.1$, $\phi = 0.1$ and $S_1 = 0.2$.

γ	S_3	Sc	$-\varphi'(0)$	
			SWCNTs	MWCNTs
0.0	0.2	1.3	0.9156	0.9236
0.3			0.9841	0.9907
0.5			1.027	1.034
	0.0		1.292	1.304
	0.2		1.027	1.034
	0.5		0.7852	0.7894
	0.2	0.8	0.8458	0.8512
		1.0	0.9247	0.9320
		1.3	1.027	1.034

bon nanotubes than the single-wall carbon nanotubes. For higher values of the curvature parameter, the radius of the cylinder decreases which reduces contact area of the cylinder with the fluid. Therefore the velocity profile increases. Variation of nanoparticle volume fraction ϕ on velocity profile is sketched in Figure 5. Velocity profile increases with an increase in nanoparticle volume fraction. Velocity distribution is higher for MWCNT. Figure 6 shows the influence of velocity slip parameter S_1 on velocity profile. The velocity profile and boundary layer thickness decrease for higher values of velocity slip parameter. Moreover velocity profile is higher in the case of MWCNT. This is due to the fact that for higher velocity slip parameter adhesive force between the wall and fluid particles decreases which provides resistance for transfer of stretching velocity to the fluid. Therefore velocity distribution decreases. The effect of ratio parameter A on temperature profile is drawn in Figure 7. Temperature and thermal boundary layer thickness decrease for higher values of ratio parameter in both (i) SWCNT (ii) MWCNT. The behavior of curvature parameter γ on temperature profile is shown in Figure 8. The temperature profile decreases near the surface of cylinder while increases away from the surface. For higher values of the curvature parameter the radius of cylinder decreases which offers less resistance. Therefore temperature near the surface of cylinder decreases. Figure 9 shows the influence of velocity slip parameter S_1 on temperature profile. Higher values of velocity slip parameter result in the enhancement of temperature and thermal boundary layer thickness. The temperature profile is higher in the case of single-wall carbon nanotubes. Behavior of the thermal slip parameter S_2 on the temperature profile is sketched in Figure 10. Temperature distribution and thermal boundary layer thickness decrease for higher values of thermal slip parameter. Heat transfer from the cylinder to the fluid de-

Table 6: Comparison of $f''(0)$ with Mahapatra and Gupta [25], Pop *et al.* [26] and Sharma and Singh [27] for various values of A when $\gamma = 0$, $\phi = 0$ and $S_1 = 0$.

A	Mahapatra and Gupta [25]	Pop *et al.* [26]	Sharma and Singh [27]	Present results
0.1	-0.9694	-0.9694	-0.969386	-0.96939
0.2	-0.9181	-0.9181	-0.9181069	-0.91811
0.5	-0.6673	-0.6673	-0.667263	-0.66726
0.7				-0.43346
0.8				-0.29929
0.9				-0.15458
1.0				0.00000

creases which results in the reduction of the temperature profile. Higher temperature was noted for the single-wall carbon nanotubes. Characteristics of the curvature parameter γ on the concentration profile is displayed in Figure 11. Concentration profile decreases near the surface of cylinder while increases away from the surface. Behavior of the solutal slip parameter S_3 on the concentration profile is visualized in Figure 12. Concentration profile decreases for higher values of the solutal slip parameter. The effect of Schmidt number Sc on the concentration profile is shown in Figure 13. Decreasing behavior of the concentration profile is noted for larger Schmidt number. The solutal boundary layer thickness decreases. Mass diffusivity decreases with an increase in Schmidt number. Therefore the concentration profile decreases.

Table 2 shows the convergence of series solutions of momentum, energy and concentration equations. We see that 13^{th} order approximations are sufficient for the convergence of momentum and concentration equations while 20^{th} order approximations are enough for energy equation in the case of SWCNTs. For the MWCNTs 10^{th} order approximations are enough for the convergence of momentum and concentration equations while 20^{th} order approximations are sufficient for the energy equation. Table 3 shows the influence of pertinent parameters on the skin friction coefficient. The skin friction coefficient increases as γ and ϕ increase, while it decreases for larger values of A and S_1 for both SWCNTs and MWCNTs. The skin friction coefficient is higher for SWCNTs when compared with MWCNTs. Table 4 presents variation of various parameters on the Nusselt number. Higher values of γ, A and smaller values of ϕ and S_2 result in enhancement of the Nusselt number for both SWCNTs and MWCNTs. The Nusselt number is higher for MWCNTs for all parameters. Table 5 explores the effects of different parameters on Sherwood number. The Sherwood number is higher for larger values of γ, Sc and smaller values of S_3 for both SWCNTs and MWCNTs. The Sherwood number is higher for MWCNTs. Table 6 shows comparison of skin friction coefficient with previous published data. The results are in good agreement.

4 Closing remarks

We have explored the characteristics of boundary layer stagnation point flow of a nanofluid past a stretching cylinder using single- and multi-wall carbon nanotubes. Heat and mass transfer are examined with slip effects. The main points of the present investigation are as follows:

- Velocity profile is higher for curvature parameter γ and nanoparticle volume fraction ϕ in the case of multi-wall carbon nanotubes compared to single-wall carbon nanotubes.
- Higher values of velocity slip parameter S_1 reduce the velocity profile and associated boundary layer thickness.
- Thermal and solutal slip parameters S_2 and S_3 result in the reduction of temperature and concentration profiles for both SWCNT and MWCNT cases.
- Temperature and concentration profiles decrease near the surface of cylinder while these decrease away from the surface of cylinder.

References

[1] S.U.S. Choi, D.A. Siginer, H.P. Wang (Eds.), FED-Vol. 231/MD 66 (ASME, New York, 1995) 99
[2] Z. Said, R. Saidur, N.A. Rahim, M.A. Alim, Energy Build. 78, 1 (2014)
[3] M.M. Rashidi, S. Abelman, N.F. Mehr, Int. J. Heat Mass Trans. 62, 515 (2013)
[4] M. Sheikholeslami, R. Ellahi, H.R. Ashorynejad, G. Domairry, T. Hayat, J. comput. Theor. Nanos. 11, 486 (2014)

[5] K. Bhattacharyya, G.C. Layek, Phys. Res. Int. 2014, 592536 (2014)
[6] M. Sheikholeslami, M.G. Bandpy, D.D. Ganji, S. Soleimani, J. Mol. Liq. 196, 179 (2014)
[7] M. Imtiaz, T. Hayat, M. Hussain, S.A. Shehzad, G.Q. Chen, B. Ahmad, Eur. Phys. J. Plus 129, 97 (2014)
[8] M. Turkyilmazoglu, ASME J. Heat Transfer 136, 031704 (2013)
[9] P.D. Weidman, V. Putkaradze, Eur. J. Mech. B/Fluids 22, 123 (2003)
[10] Y.Y. Lok, J.H. Merkin, Int. J. Thermal Sci. 59, 186 (2012)
[11] K.L. Hsiao, Appl. Thermal Eng. 27, 1895 (2007)
[12] K. Bhattacharyya, K. Vajravelu, Commun. Nonlinear Sci. Numer. Simulat. 17, 2728 (2012)
[13] M. Turkyilmazoglu, I. Pop, Int. J. Heat Mass Trans. 57, 82 (2013)
[14] T. Hayat, Z. Hussain, M. Farooq, A. Alsaedi, M. Obaid, Int. J. Nonlinear Sci. Numer. Simulat. 15, 77 (2014)
[15] S. Mukhopadhyay, Meccanica 48, 1717 (2013)
[16] S.J. Liao, Homotopy analysis method in non-linear differential equations (Springer and Higher Education Press, Heidelberg, 2012)
[17] M. Turkyilmazoglu, Commun. Nonlinear Sci. Numer. Simulat. 17, 4097 (2012)
[18] O.A. Beg, M.M. Rashidi, T.A. Beg, M. Asadi, J. Mech. Med. Biol. 12, 1250051 (2012)
[19] S.A. Shehzad, A. Alsaedi, T. Hayat, Braz. J. Chem. Eng. 30, 897 (2013)
[20] S. Abbasbandy, M. Jalil, Numer. Algor. 64, 593 (2013)
[21] T. Hayat, A. Qayyum, F. Alsaedi, M. Awais, A.M. Dobaie, Eur. Phys. J. Plus 128, 85 (2013)
[22] M.M. Rashidi, B. Rostami, N. Freidoonimehr, S. Abbasbandy, Ain Shams Eng. J. (2014) in press.
[23] T. Hayat, A. Shafiq, A. Alsaedi, Plos one 9, e83153 (2014)
[24] W.A. Khan, Z.H. Khan, M. Rahi, Appl. Nanosci. 4, 633 (2014)
[25] T.R. Mahapatra, A. Gupta, Heat Mass Trans. 38, 517 (2002)
[26] S. Pop, T. Grosan, I. Pop, Tech. Mech. 25, 100 (2004)
[27] P. Sharma, G. Singh, J. Appl. Fluid Mech. 2, 13 (2009)